Dipole Moment Reversal in a Polar Organic Monolayer Probed by Sum and Difference Frequency Spectroscopy

Natalia García Rey[1,a,*], *Marco Sacchi*[2,b], *Stephen J. Jenkins*[2] *and Heike Arnolds*[1,*]

[1]Surface Science Research Center, Department of Chemistry, University of Liverpool, Oxford Road, Liverpool L69 3BX, UK.

[2]Department of Chemistry, Cambridge University, Lensfield Road, Cambridge CB2 1EW, UK

[*] E-mail address: ngarciar@illinois.edu

[*] E-mail address: Heike.Arnolds@liverpool.ac.uk

ABSTRACT

We investigate the adsorption of pyridine on Cu(110) in ultra-high vacuum with a combination of work function measurements and femtosecond infrared-visible sum and difference frequency generation (SFG/DFG). A monolayer of pyridine substantially reduces the work function by 2.9 eV due to the large pyridine dipole. We perform density functional theory (DFT) calculations that provide us with a dipole moment change upon adsorption in very good agreement with the experimental results. The pyridine dipole strongly enhances the sum frequency response of the surface electrons, but surprisingly reduces the surface difference frequency signal. We propose a model based on the static electric field-induced nonlinear optical response generated by the collective electric field of the adsorbate layer. The pyridine dipole switches direction from the ground to the excited electronic state, as charge moves from nitrogen to the ring. SFG can then be enhanced by the electric field of adsorbed pyridine in its ground electronic state, while the 2.33 eV incident photon in DFG excites electrons into the pyridine LUMO, which reverses the electric field in the adsorbate layer and reduces the nonlinear optical response. The model is verified by 2.33 eV pump – SFG probe spectroscopy, where the pump pulse is found to reduce the surface electron response on a subpicosecond timescale. This demonstrates the potential to manipulate the work function in organic electronic devices by photon-induced dipole moment reversal.

INTRODUCTION

Work function tuning of metallic interfaces by adsorption of molecules is a key tool to change charge carrier injection barriers in organic electronic devices, for example self-assembled monolayers of π-conjugated molecules with different head and tail groups adsorbed on noble metals[1]. Pyridines in particular have proved desirable as an anchoring group as they have a high affinity to metal surfaces and because adsorption-induced charge arrangements extend beyond the immediate anchor group into the backbone[2]. Pyridine itself possesses a large molecular dipole of 2.2 D, which allows a good degree of work function tunability, as recently shown by 3 eV change observed on the transparent conductor ZnO[3].

The collective electric field created by such polar adsorbates is known to have a major effect on excited states, adsorption energy, adsorption site and long-range order[4-7]. While extrinsic electric fields have been used to manipulate energy level alignment and therefore electron transfer or reaction rates in many areas of chemistry[8], it is yet unknown to which degree we can manipulate intrinsic fields of an adsorbate layer to achieve similar effects at interfaces.

Second-order nonlinear optical spectroscopy has emerged as a frequent solution to obtaining molecular-level information from interfaces, as its selection rules render it interface-specific. In order for two incident photons to combine in a medium to create a photon at the sum frequency, a lack of inversion symmetry is required, which is a defining characteristic of any interface. Sum frequency generation (SFG) has therefore been widely used to study the interaction of molecules with interfaces, ranging from adsorbates on metal surfaces[9-10], organic films [11-12], biological interfaces [13-14] to gas-liquid interfaces [15-16].

Static electric fields at interfaces can also be probed by SFG, when the two time-varying fields of the incident waves combine with a static electric field through a cubic susceptibility. This effect

is now commonly used in nonlinear optical investigations of electrochemistry to determine the point of zero charge of the interface[17-18] or to control the nonlinear optical signal[19]. As the so-called Eisenthal $\chi^{(3)}$ technique it is also frequently used to monitor interfacial fields at dielectric interfaces, for example to determine local pH or Debye lengths[20-24]. However, the electric field created by pre-aligned polar molecules at an interface has been largely ignored as a signal source, likely because the electric fields created by charged adsorbates or externally applied are normally much larger than the field created by the molecular dipoles.

Here we take account of the dipolar nature of the adsorbate and the collective electric field created to demonstrate the link between work function changes and changes in the second-order nonlinear optical response. To this end, we measure the work function change during the adsorption of pyridine on Cu(110) with a Kelvin probe and characterize the adsorbate layer by vibrational sum frequency generation in the C-H stretching region. In order to investigate the adsorbate electronic structure, dipole and geometry conformation, we perform density functional theory calculations (DFT) of pyridine chemisorbed on a (2 × 2) Cu(110) unit cell. The results of the DFT calculations help us to rationalize the charge transfer and induced change in the molecule-surface dipole moment. In addition, we monitor the nonlinear optical response of the surface electrons during pyridine adsorption using both sum frequency (1.55 eV + 0.38 eV=1.93 eV) and difference frequency (2.33 eV – 0.38 eV = 1.95 eV). Both sum and difference frequency signals change in a similar manner to the work function, but SFG is enhanced by adsorbed pyridine, while DFG is suppressed. In addition we observe that a 2.33 eV pump pulse reduces both nonresonant and resonant sum frequency responses. We propose an electric field-induced effect, which switches sign from SFG to DFG, because the 2.33 eV photon involved in DFG transfers charge to the pyridine ring and reverses the molecular dipole.

EXPERIMENTAL AND COMPUTATIONAL METHODS

Ultra-High Vacuum-Sum Frequency Generation Spectrometer

We used an amplified, 10 Hz repetition rate Ti:Sapphire femtosecond laser system (Spectra-Physics, TSA-10), generating pulses of 150 fs pulse width and 6 mJ energy. Part of the amplifier output was used to pump an optical parametric amplifier (TOPAS, LightConversion) for tunable mid-IR generation with a typical bandwidth of 150 cm^{-1} and part was spectrally narrowed with a homebuilt stretcher (spectral width 5.3 cm^{-1}) [25] or an etalon (SLS Optics Ltd., 7.2 cm^{-1} spectral width) [26]. The sum frequency generated by the interface was directed into a 0.3 m spectrograph (ActonSpectraPro 300i) with ICCD detection (Andor iStar). For one spectrum, typically the signal from 1000-2000 shots was accumulated with full 0.7 cm^{-1}/pixel resolution. A bandpass interference filter centered at 650 nm (± 80 nm) (Edmund Optics) was used to filter the visible beams. All beams were p-polarized.

Ultra-High Vacuum techniques and sample preparation

Work function and vibrational sum frequency generation measurements were carried out in an ultra-high vacuum (UHV) chamber at a base pressure of $3x10^{-10}$ mbar and crystal base temperature of 100 K. The Cu(110) crystal was cleaned by repeated cycles of 500 V Ar^+ ion sputtering and 650 K annealing until a sharp LEED (1×1) pattern was obtained. The sample cleanliness was confirmed by reproducible sum frequency spectra and temperature programmed desorption (TPD) at 2 Ks^{-1} recorded with a quadrupole mass spectrometer (MKS Microvision-2).

Pyridine (anhydrous, 99.8%, SigmaAldrich) was dosed from the liquid after several freeze-pump-thaw cycles, through a 20 cm long stainless steel tube to provide a degree of directional dosing. Dosing about one monolayer at 100 K typically took 20 minutes at m/z 52 partial pressure of around 10^{-10} mbar. The m/z 52 corresponds to the fragmentation of pyridine molecular ions to

form $[C_4H_4]^{+\cdot}$, formed in higher numbers than the parent ion at m/z 79. A Kelvin probe (Besocke Delta PHI GmbH) was used to monitor the change in work function as a function of adsorbate coverage. To convert from dosed pressure to surface coverage, the m/z 52 signal was integrated over time and calibrated by TPD.

Density Functional Theory

The Perdew-Wang 91 exchange-correlation functional [27] was employed to calculate the ground state energy of the system. The plane waves basis set was expanded up to a 340 eV kinetic energy cut-off, tested to ensure convergence of the basis set [28]. The Brillouin zone was sampled with a 4×4×1 Monkhorst-Pack k-point grid [29]. The electron energy is converged to 10^{-6} eV and the force tolerance in the geometry optimization is set to 0.05 eV/Å.

To calculate the dipole of a (2x2) pyridine layer, we employed the so called "symmetric double layer" approach, consisting of modelling the pyridine on Cu(110) surface by a symmetric slab of 7 layers of Cu atoms in which the middle 3 layers of copper are fixed and the top and bottom 2 are free to relax. Pyridines on the top and bottom layer were mirror images. This approach is computationally more demanding than a normal "single sided" calculation, but has the advantage of eliminating all the possible artefacts due to the presence of a strong dipole moment in the periodically repeated cell.

RESULTS AND DISCUSSION

Work function of pyridine on Cu (110)

Pyridine adsorbs through the nitrogen lone pair on Cu(110)[30] with its molecular axis considered to be upright at all but the lowest coverages[31-33]. With the nitrogen lone pair pointing towards the surface, the molecular dipole opposes the metal surface dipole and reduces the work function.

Figure 1 shows the work function change induced by pyridine adsorption at 100 K, recorded during background dosing at a pressure of around $5 \cdot 10^{-9}$ mbar. Stepwise annealing of pyridine whilst monitoring $\Delta\phi$ and m/z 52 partial pressure allows us to assign the work function minimum to a saturated first layer with nominal 1 ML coverage (see TPDs in Fig. 4 (c)). This layer possesses an absolute coverage of 40% relative to the copper surface as determined by XPS[34], corresponding to $4.34 \cdot 10^{18}$ m^{-2} surface density. The clean Cu(110) work function has been determined as 4.46 eV [35]

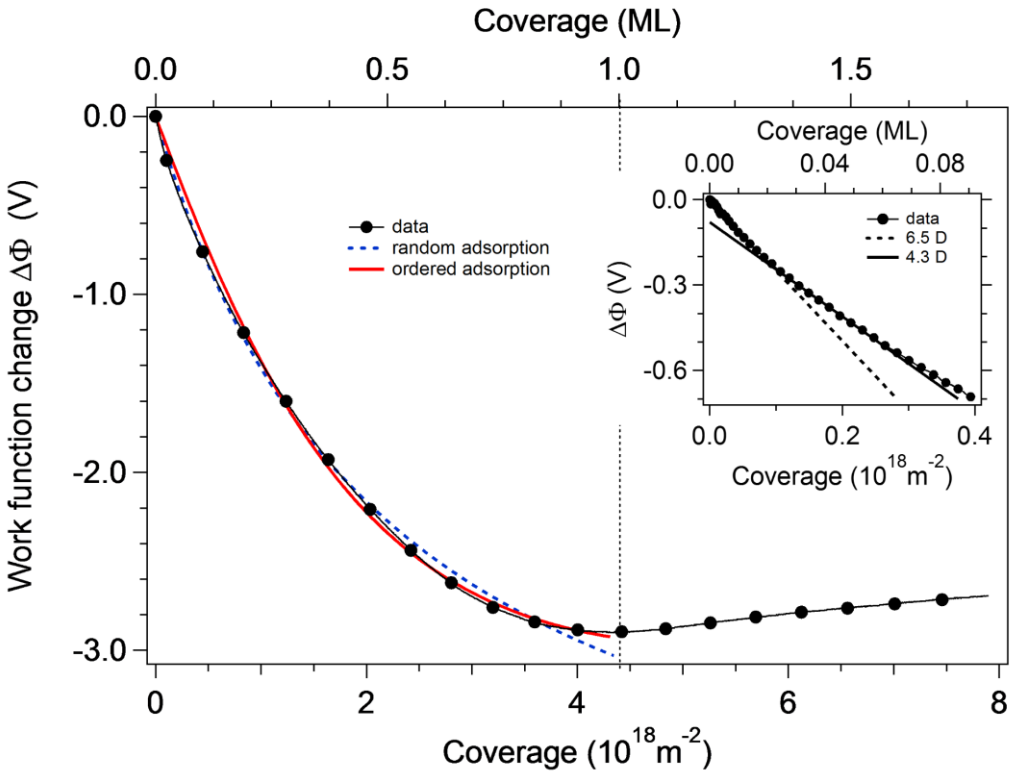

Figure 1. Work function change of pyridine/Cu(110) measured during continuous dosing (circles show every 100th data point). Red and blue lines are fits to the data assuming either random adsorption (blue) or ordered adsorption (red). The inset shows linear fits to the work function change for very low coverages (circles show every 5th data point).

in the literature and as 4.47 ± 0.05 eV from our own UPS experiments, which means a surface covered by a monolayer of pyridine has a work function of only 1.6 eV.

For comparison, pyridine adsorption on Cu(111) only reduces the work function by 2.3 eV[36]. The difference could be caused by packing density, surface structure or surface order as modified by dosing pressure. For example, on platinum surfaces a reduction in the dosing pressure from $2 \cdot 10^{-7}$ torr to 10^{-8} torr leads to an additional decrease in the work function by between 0.2 and 0.4 eV[37]. The reduction of the work function by 2.9 V is large, but comparable to the effect of pyridine on several other metal surfaces (listed in the Table S1 in the supporting information) and very similar to the 3 eV reduction recently measured on ZnO(10-10)[3].

We can extract the initial adsorbate dipole moment μ from the slope of the work function at low coverages, before adsorbates start interacting, using the expression

$$\mu = \frac{\varepsilon_0 \Delta V}{n}, \qquad (1)$$

where ΔV is the measured work function change in volts, n is the adsorbate density in molecules per m^2 and ε_0 is the permittivity of free space. The inset to Fig. 1 shows that the slope changes at a coverage of only 0.02 ML or 10^{17} m^{-2}, corresponding to an intermolecular distance of around 3 to 4 nm. Below this coverage, the pyridine dipole moment is 6.5 D, while just above this coverage, the slope corresponds to 4.3 D. These values are three, respectively two times as high as the pyridine gas-phase dipole moment of 2.15 D [38]. Such enhancement is caused by image dipoles in the metal surface and has been seen in other cases, for example carbon monoxide (0.112 D in the gas phase[39] versus 0.9 D on Pt(111)[40]).

The change in slope occurs in a coverage region where scanning tunneling microscopy detects a transition between two pyridine species with different apparent heights and different resonances

in the unoccupied density of states, which were assigned to tilted and fully upright species[32]. Both species bind through the nitrogen atom, but the tilted species can in addition interact through its π electrons. We accordingly assign the higher initial dipole moment to the tilted species and the lower one to the fully upright species. This switch from tilted to upright has been seen for other surfaces. On Cu(111), the initial steep decline in the work function up to 0.6 ML was assigned to a flat-lying species with a slower decrease in Φ seen at higher coverages for the N-bonded species as a result of a balance between pyridine dipole moment, charge transfer and mutual depolarisation at high coverages[36]. The existence of two species was also proposed for pyridine adsorption on Ag(110), where a flat species is thought to exist at low coverages, changing to a tilted species at higher coverages with a factor 4 difference in the work function change per molecule[41]. The larger dipole of a tilted or flat pyridine molecule can arise from the so-called cushion effect, where the electron cloud of the adsorbate pushes back the surface electrons and thereby lowers the work function [42].

In order to fit the work function change caused by the pyridine layer, we use the standard electrostatic derivation[43-44]. The dipole moment of a single dipole within an array of dipoles on a metal surface is modified by the electric field generated by its own image and the collective field of all the other dipoles and their images. This can be described by

$$\mu = \mu_0 + \alpha E = \mu_0 + \alpha_{zz} E, \qquad (2)$$

where μ_0 is the dipole in the limit of zero field and α is its polarizability. Since the metallic surface effectively shields all parallel dipole components, we can replace α by α_{zz}. The electric field seen by the dipole in (2) amounts to

$$E = \frac{\mu}{4d^3} - \mu S(n) = \frac{\mu}{4d^3} - \mu\left(\sum_{R_J}{}' \frac{1}{R_J^3} + \frac{1}{\left(R_J^2 + 4d^2\right)^{3/2}} - \frac{12d^2}{\left(R_J^2 + 4d^2\right)^{5/2}} \right), \quad (3)$$

where the first term is the field created by the image dipole (image distance *d*) and the second term constitutes the sum over all other dipoles and their images and respective interactions for an array of density *n* (lattice vector R_J). An analytical solution for a hexagonal array was first presented by Topping [45], who found that $S(n)=8.89n^{3/2}$.

The presence of the metal surface thus enhances the adsorbed dipole and in the limit of zero coverage, the adsorbed dipole moment is given by

$$\mu = \frac{\mu_0}{1 - \frac{\alpha_{zz}}{4d^3}}. \quad (4)$$

The work function change can now be fitted to

$$\Delta\Phi = -\frac{n\mu_0}{\varepsilon_0} \cdot \frac{1}{\left(1 + \alpha_{zz}\left[S(n) - \frac{1}{4d^3}\right]\right)}. \quad (5)$$

The dipole sum S(n) can be calculated for an ordered dipole array, although little detail is known about ordered structures of pyridine on Cu(110). LEED patterns of (4x3) symmetry for the pyridine monolayer and (5x3) at slightly lower coverages have been observed[31], but these must contain around 5 molecules in the unit cell in order to reproduce the coverage of 0.4 per Cu unit cell found by XPS[34]. For an image distance of 2.14 Å (see below), a (2x2) arrangement on Cu(110) would correspond to a dipole sum of S(0.25 ML) = 0.039 $Å^3$, while a c(2x2) arrangement would yield a dipole sum of S(0.5 ML) = 0.082 $Å^3$. The dipole sum is normally extrapolated between a known ordered structure and zero coverage, although the functional dependence on coverage depends on

how the adsorption proceeds[43]. If there is an ordered adsorption throughout, which can be modelled as a continuously shrinking lattice size with increasing coverage, then the dipole sum will be proportional to the coverage to the power of 3/2, while a random filling of adsorption sites leads to a linear dependence on coverage. We fitted the work function with both coverage dependencies as shown in Fig. 1. As expected, random adsorption provides a better description of the data at low coverages, while ordered adsorption describes them better near monolayer saturation. The results of the fit are not changed much by the model chosen.

Since the dipole sum depends on the image distance, we cannot independently determine both from the fit. We can estimate the image distance from known parameters. If we place pyridine's dipole at the center of the molecule, then its position is 1.84 Å above the nitrogen atom, which in turn is 2 Å above a copper atom[34]. Since the image plane is located 1.7 Å outside the last atomic layer on Cu(110)[46], the theoretical distance between the point dipole and its image is 2.14 Å. With the pyridine gas phase dipole moment μ_0=2.15 D, a fit then yields a dipole sum of 0.036 Å^3, relatively close to the value calculated for a (2×2) layer, and a polarizability of α=19.1 A^3. Pyridine's gas phase polarizability is 9.3 Å^3, which is an angle-averaged value, corresponding to the trace of the polarizability tensor = $(\alpha_{xx} + \alpha_{yy} + \alpha_{zz})/3$. For pyridine, α_{xx} and α_{zz} are approximately equal and three times the value of α_{yy}, so the angle-averaged gas phase value corresponds to $\alpha_{zz} \approx$ 12 Å^3. The polarizability of pyridine is therefore enhanced about 50% by adsorption. Inserting the fitting results into eqn. (4) produces a dipole moment in the limit of zero coverage of 4.2 D.

We have used DFT to calculate the dipole moment of a (2x2) layer of pyridine on Cu(110), which results in a value of 2.37 D. A (2x2) layer has an absolute coverage of 0.25 molecules per surface unit cell which corresponds to 0.25/0.4=0.625 ML relative coverage and a surface density of $2.69 \cdot 10^{18}$ m^{-2}. At this coverage we measured a work function change of ΔV=-2.54 eV= $n\mu/\varepsilon_0$,

corresponding to an average μ=2.51 D. There is a remarkably good agreement (within 6%) between the experimentally measured dipole and the results of the DFT calculation.

Since pyridine bonds in a vertical orientation on Cu(110), the main bonding mechanism involves a strong hybridisation of the σ-like HOMO and the π-like HOMO-2 with the copper d_{y2} and d_{yz}-type orbitals[47]. We calculate the π_1 orbital ($1a_2$) to be at E_F-4 eV, the π_2 ($2b_1$) at E_F-4.9 eV and the σ_1 orbital ($7a_1$) at E_F-5.2 eV. Our UPS spectra (Fig. S1 in the supporting information) confirm that changes occur in the occupied density of states in the energy range of 3 to 6 eV below E_F. Other DFT studies on ZnO(10-10) and Au(111) have shown that both the pyridine molecular dipole as well as charge transfer to the surface (the so-called bond dipole) contribute to the work function decrease. On gold, the bond dipole contributes about a third of the total work function change[2], while molecular and bond dipoles were found to contribute equally on zinc oxide.

Even though the pyridine dipole moment decreases strongly in a more densely packed adsorbate layer, it is still large enough to create strongly repulsive adsorbate-adsorbate interactions, which are the origin of the continuous downshift of the maximum pyridine desorption temperature with coverage and were determined to amount to 0.16 eV/ML for a zero-coverage desorption energy of 0.97 eV [31].

We can finally estimate the electric field in the pyridine layer from the coverage-dependent dipole moment.

$$E = \mu\left(\sum_{R_J}{}' \frac{1}{R_J^3} + \frac{1}{\left(R_J^2 + 4d^2\right)^{3/2}} - \frac{12d^2}{\left(R_J^2 + 4d^2\right)^{5/2}}\right) \qquad (6)$$

At saturation coverage, we thus obtain a field of 10^9 V/m, which is of similar magnitude as electric fields induced by fcc adsorbates such as NO and CO in neighboring atop sites on Pt(111)[7].

Sum frequency spectroscopy of pyridine on Cu(110)

The vibrational sum frequency spectra of pyridine in the C-H stretching region with increasing pyridine coverage were also acquired during continuous background dosing and are shown in Fig.2. Spectra normalized by the nonresonant response of the bare copper surface are shown in Fig. S2 in the supporting information. Total coverage was determined at the end of dosing from integrating TPD traces, since the second layer of pyridine desorbs in a sharp peak below 160 K. Coverage for individual spectra was then scaled by assuming a constant sticking coefficient during adsorption at 100 K.

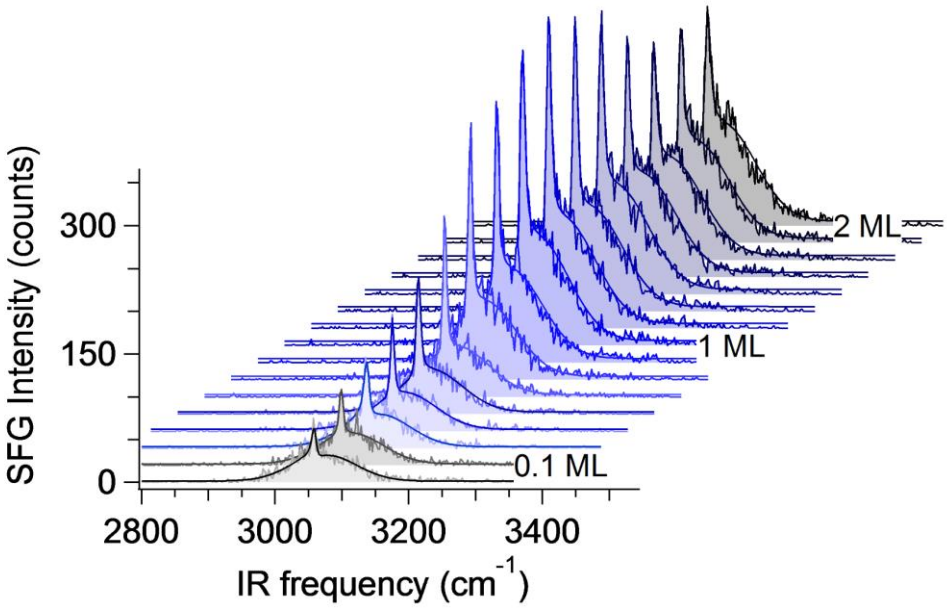

Figure 2. Sum frequency spectra as a function of pyridine coverage on Cu(110).

Sum frequency generation is a second order nonlinear process produced when two intense laser beams impinge on the interface between two media. If the frequencies of the driving fields excite the surface electrons and a single vibrational mode in adsorbates, we can express $\chi^{(2)}$ as [48-49]:

$$\chi^{(2)} = \chi^{(2)}_{NR} + \chi^{(2)}_{RES} = A_{NR} \cdot e^{i\varphi} + \frac{A_R}{(\omega_{IR} - \omega_R) + i\Gamma_R} \qquad (7)$$

where A_{NR} is the strength of the vibrational nonresonant (NR) susceptibility of the surface with phase φ, A_R is the product of dynamic dipole moment and polarizability for the vibrational resonance, ω_R and Γ_R are the frequency and width of the molecular resonance. The sum frequency intensity depends on the number and the layer-order of adsorbed molecules. For a single vibrational resonance, two solutions exist which only differ in the value of the phase φ and resonant amplitude A_R[50]. Apart from the change in tilt angle at very low coverage, the bonding between pyridine and copper remains unchanged and therefore Fig. 3 shows the solution where the phase only has a small dependence on coverage. The second solution (Fig. S3 in the supporting information) shows a phase change of 130^0, which could indicate the appearance of an electronic resonance. This resonance would not be related to interband or surface state transitions, as both upconversion photon energy (1.55 eV) and sum frequency photon energy (1.93 eV) are too low in energy, but could be caused by the pyridine LUMO shifting into resonance with increasing coverage. This will be discussed further below. All fits were carried out in IgorPro 6.1.2. (from Wavemetrics), which uses a Levenberg-Marquardt algorithm.

Only a single vibrational mode is found in the C-H stretching region, which we assign to the ν_2 vibration, where all C-H bonds vibrate in phase. The two other allowed totally symmetric modes, ν_{20a} and ν_{13} have much smaller predicted intensities in Infrared and Raman and are not seen in the monolayer (see Table S2 in the supporting information for details). The intensity of the resonance increases monotonically until 1 ML and then decreases slightly. This can have a number of reasons, for example, a shorter vibrational lifetime or inhomogeneous distribution of adsorption sites as

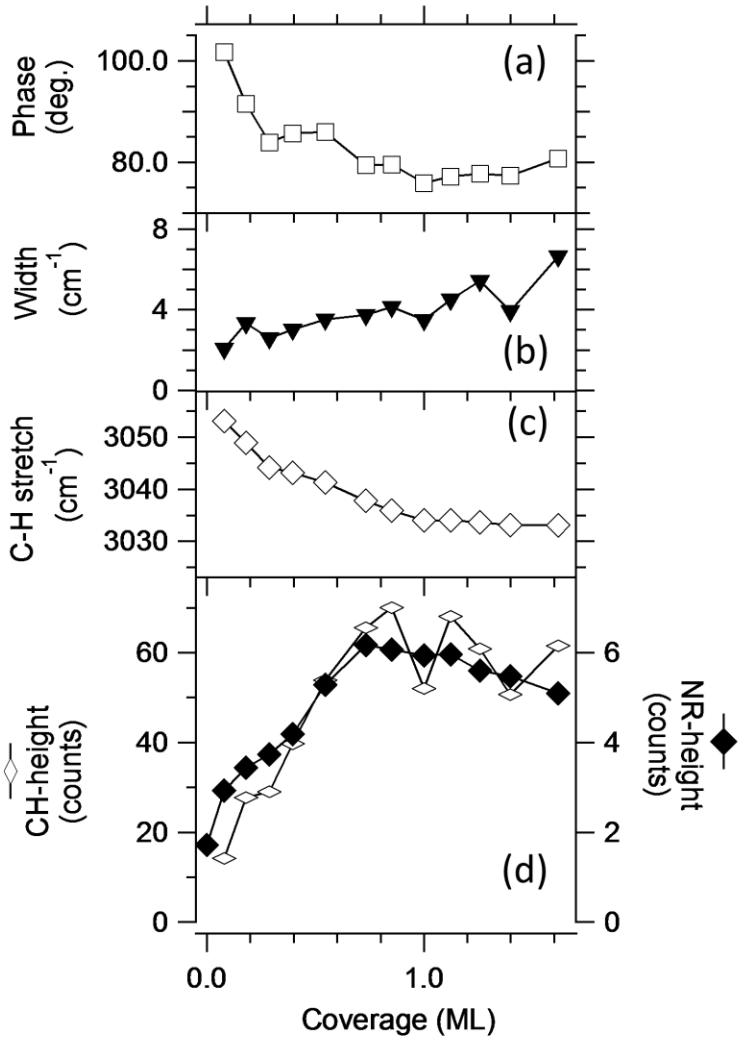

Figure 3. SFG spectral parameters of the CH- stretch (RES): (a) phase, (b) width, (c) frequency and (d) intensity (left axis), and (d) NR contribution intensity (right axis) of the pyridine adsorbed on Cu(110) as a function of coverage.

indicated by the increase in bandwidth above 1 ML. The first pyridine layer on the contrary is highly ordered as confirmed by very narrow vibrational line widths of around 4 cm^{-1}. Depolarization or structural changes in the first layer by the second layer can also explain a reduction in amplitude. Even at our low dosing rate, we cannot exclude that a second layer forms in patches before the first layer is saturated. The C-H stretching frequency of pyridine shows a 19

cm^{-1} red shift with increasing coverage (Fig. 3(c)). A slightly smaller downward frequency shift was also observed by RAIRS [51]. Dynamic dipole-dipole coupling is unlikely to affect the spectra, as a mixed isotope study of pyridine adsorption on a gold electrode failed to find any discernible frequency shifts or intensity changes with changing isotope composition[52]. Given the magnitude of the electric fields deduced from the work function measurement, the frequency shift could be caused by a Stark effect. A small effect of 6 cm^{-1}/V for the C=C ring stretch has been reported for pyridine adsorbed on a gold electrode immersed in 1 M NaF, which was explained either by a weak Stark effect or by a change in charge density on the nitrogen lone pair with electrode potential[53]. The Debye length of 1 M NaF is 0.3 nm at room temperature, therefore the electric field corresponding to 1 V externally applied is $3 \cdot 10^9$ Vm^{-1}, very similar to our calculated value. Raman spectra have been calculated for pyridine adsorbed on silver clusters as a function of external field and only very small Stark effects have been found for the totally symmetric modes detected here[54], so the red shift more likely arises from chemical effects.

Surface electron response probed by sum and difference frequency spectroscopy

The broad underlying peak in the spectra reflects the spectral width of the incident infrared pulse and is caused by the non-resonant response of the surface electrons to the exciting fields. It shows an unusually strong increase starting from the lowest coverages and a small decrease in the multilayer range. It mirrors the coverage-dependence of the work function, as a comparison between Fig. 1 and Fig. 3(d) reveals. The second-order response of the surface has often been observed to change in opposite direction to the work function upon alkali or molecular adsorption on metal surfaces[55-57]. To better understand the link between work function and nonlinear optical response, we measured difference frequency generation between a 2.33 eV upconversion beam,

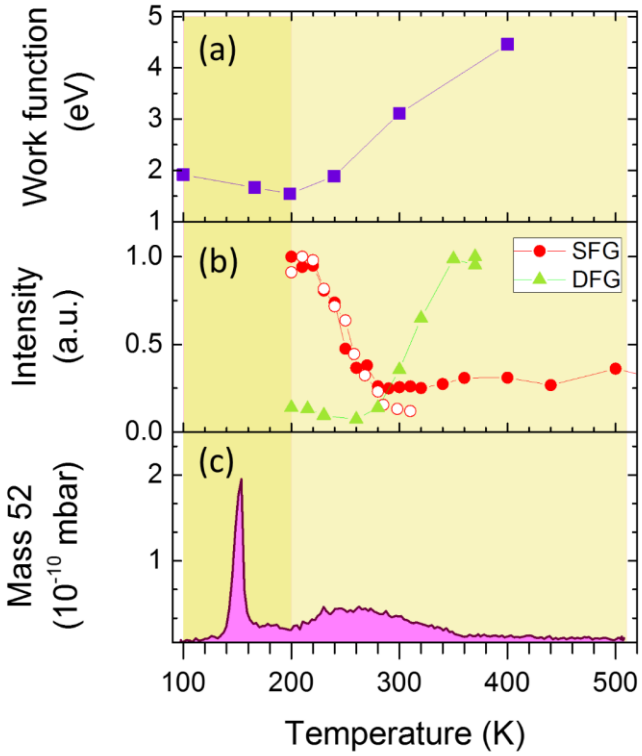

Figure 4. Following NR signals with DFG and SFG as a function of annealing temperature. (a) Work function measured during stepwise annealing (filled squares). (b) RES (open circles) and NR (filled circles) signals for SFG and NR signal (filled triangles) for DFG. (c) TPD recorded at 2 K/s. At 200 K, the pyridine coverage is 1 ML.

and the same IR at 0.38 eV, which results in an emitted photon at 1.95 eV. This way, two of the three photons in the DFG and SFG processes are still at the same energy and we are able to explore whether any electronic excitations underlie the increased response. The DFG signal is much larger than the SFG signal, because the visible photon can excite interband transitions. As the 2.33 eV beam is a broadband pulse, there is insufficient spectral resolution to detect the pyridine vibrational resonance, but changes in surface response can be easily detected. The pyridine resonant response is negligible as a comparison of free-induction-type measurements on bare copper and 1 ML pyridine shows (see Fig. S4 in the supporting information). We record the coverage dependence

by dosing a slight multilayer of pyridine and stepwise annealing and observing SFG, DFG and work function changes in subsequent experiments. The results are shown in Fig. 4.

Surprisingly, pyridine adsorption has the opposite effect on sum and difference frequency signals, as it enhances SFG and reduces DFG. To understand the different responses better, we look at the most general expression for the second order response of a noble metal surface[48]. Possible sources of a second-order surface polarizability on Cu(110) are free electrons (intraband transitions) or bound electrons (interband and electrons in surface-confined states). Free electrons can contribute both via a quadratic susceptibility and a cubic susceptibility in the presence of an electric field and we can write the total polarizability as:

$$P^{(2)}_{total}(\omega = \omega_1 \pm \omega_2) = \chi^{(2)}_{NR} E(\omega_1) E(\omega_2) = \left(\chi^{(2)}_{free} + \chi^{(3)}_{free} E_{DC} + \chi^{(2)}_{bound}\right) E(\omega_1) E(\omega_2) \qquad (8)$$

Using the jellium approximation, the contribution from free electrons can be shown to be real valued terms, while electronic resonances such as interband and surface state transitions can be approximated near resonance as imaginary terms whose magnitude increases in the corresponding spectral range:

$$\chi^{(2)}_{NR} = \alpha + \delta E_{DC} + \sum_n \frac{\beta_n}{\omega - \omega_n \pm i\Gamma_n} \approx \alpha + \delta E_{DC} + \sum_n i\gamma_n \qquad (9)$$

The phase generally attached to the nonresonant susceptibility in the sum frequency equation (7) accounts for the fact that the measured signal is also influenced by the Fresnel factors, which are complex numbers for a metal with its complex refractive index. We will now discuss the various contributions in eqn (9) in turn.

Free electrons

A close relationship between work function and a changing second harmonic or nonresonant sum frequency response is expected when the free electron response of the metal dominates[17, 57].

Changes in the nonlinear response term α can then be understood as adsorbate-induced changes in the free electron density at the surface due to charge transfer between adsorbate and metal, such that electron withdrawing adsorbates like CO and oxygen tend to reduce the nonresonant response, while electron donating adsorbates such as ammonia or alkalis enhance it. This is clearly a very appropriate explanation for adsorbed alkalis, but becomes doubtful for electron donating adsorbates such as pyridine, which form a covalent, highly localized bond with a copper atom. The reduction of the DFG signal by pyridine adsorption confirms that a change in free electron density is unlikely to be the source of the nonresonant signal changes, as no strong wavelength dependence is expected.

Bound electrons

The outgoing photon energies in SFG and DFG are very similar at 1.93 and 1.95 eV, respectively, and could be resonant with either copper interband transitions or the surface state transition at the $\overline{\Gamma Y}$ point at about 2.1 eV, which has been investigated in detail with SHG[58]. This surface state transition causes a ten-fold enhancement of the SHG signal when the incident photon matches the resonance. As our beams are incident about 60^0 away from the $\overline{\Gamma Y}$ direction, we would not expect this transition to contribute much to the bare copper signal. Pyridine adsorption on other noble metal surfaces is also known to quench the surface state, as shown by inverse photoemission for Cu(111) and Au(110)[59]. We therefore consider it unlikely that the surface state transition contributes significantly to either SFG or DFG signals.

Interband transitions likely contribute to DFG with an incoming photon energy of 2.33 eV, but probably only have a minor influence on SFG with the emitted photon at 1.93 eV. A second harmonic scan from 1 to 2.5 eV on Cu(111) showed that the response cannot be completely described by free electrons[60], but the available literature generally agrees that interband transitions

do not play a role for photon energies below 2 eV[61-62]. Pyridine adsorption does affect the d-band density, but as our own UPS data show (SI), changes only occur more than 3 eV below E_F, out-of-reach of the DFG photon energies.

Transitions between E_F and unoccupied pyridine-related states could potentially contribute to the nonlinear surface susceptibility. In the gas phase, pyridine possesses a negative electron affinity and the LUMO is found at 0.6 eV above the vacuum level. For multilayer pyridine, 2-photon photoemission and inverse photoemission also detect a LUMO above the vacuum level[36, 59]. For monolayer pyridine though, a weak signature was found below E_{vac} at around E_F+1.5 eV, which was assigned to a π^* state, stabilized by image charges[36]. Similarly, scanning tunneling spectroscopy of upright, N-bonded pyridine on Cu(110) detects a resonance at 2.3 eV above E_F[32]. While the precise coverage was not reported, data were only shown for up to $3.5 \cdot 10^{17}$ m^{-2} (ca 0.08 ML), where the work function is around 3. 8 eV. This π^* state will shift closer to the Fermi level with decreasing work function/ increasing coverage and could conceivably come into resonance with the SFG photon at 1.93 eV. This would lead to a gradual enhancement of the sum frequency signal by adding an imaginary term γ to the real-valued susceptibility in eqn. (8). Indeed, this could explain the very large phase change observed in one of the sum frequency solutions of eqn. (6) to the data in Fig. 3a. An additional electronic resonance could then simultaneously reduce the interband DFG signal γ_{inter}, if it possesses a different phase.

However, we consider this an unlikely explanation for a number of reasons. About a third of the large phase change seen in the second solution of the sum frequency equation occurs above 0.7 ML, where the work function changes by less than 0.2 eV. Since we would expect the pyridine LUMO to shift in a similar manner to the work function, although not necessarily parallel to it, there appears no physical basis for such a large phase change caused by an electronic resonance.

If this was the correct solution, then a much simpler explanation would be an increasing contribution from multilayer pyridine, which could conceivably show a different phase, as it does not bind directly to copper.

Regarding the reduction of the interband DFG signal by an out-of-phase electronic resonance, we need to account for the tensorial nature of $\chi^{(2)}$ and the corresponding complex Fresnel factors. The susceptibility tensor for an excitation from the Fermi level into the pyridine π^* state should be dominated by the zzz tensor element, as we are transferring charge normal to the surface. The copper surface with its two-fold symmetry, possesses 7 tensor components which contribute to a signal measured in ppp polarization. In addition to χ_{zzz}, the following elements also contribute: χ_{xxz}, χ_{yyz}, χ_{xzx}, χ_{yzy}, χ_{zxx}, χ_{zyy}. Copper is highly reflective in the mid-IR, which means the Fresnel factors in surface-normal direction are substantially larger than in surface-parallel directions, therefore tensor components other than χ_{xxz}, χ_{yyz} and χ_{zzz} can be neglected. For SFG, the Fresnel factor for χ_{zzz} is 16 × larger than for χ_{xxz} and χ_{yyz}, while for DFG it is still 9 × larger. No polarization-dependent study has been carried out to determine the $\chi^{(2)}$ tensor components of Cu(110) in the range of interband transitions, while a calculation of the Cu(001) second harmonic response indicates comparable magnitudes of χ_{xxz}=χ_{xzx} and χ_{zxx} tensor elements above 2 eV with negligible values for the χ_{zzz} element[63]. Despite the bias from the Fresnel factors, this indicates that χ_{xxz} and χ_{yyz} can make substantial contributions to the nonlinear optical response of copper in DFG. The complex Fresnel factors shift the contribution from χ_{xxz} by 65° compared to χ_{zzz} and the one from χ_{yyz} by 90° compared to χ_{zzz}.

Since each tensor element is accompanied by a different complex Fresnel factor, near cancellation of the interband susceptibility by a molecular electronic susceptibility would seem

fortuitous. We therefore consider it unlikely that a molecular electronic resonance could lead to the strong signal reduction as seen in Fig. 4 (b).

Static field at the interface

Charge transfer from the copper surface into the pyridine LUMO by the femtosecond 2.33 eV pulse involved in DFG could however have a different effect on the layer, namely it could lead to a transient increase of the work function. The pyridine dipole direction in the ground state is dominated by the nitrogen lone pair. Excitation of electrons into the LUMO will migrate charge to the pyridine ring, which reverses the dipole[64]. For pyridine in a benzene host single crystal, the change of dipole moment from the ground state to the excited state was measured as 2.6 D[65]. Since the gas phase ground state dipole moment of pyridine is 2.15 ± 0.05 D [38], the excited state dipole moment is -0.45 ± 0.05 D. This reversed dipole would enhance the surface work function and change the sign of the static electric field in eqn. (8-9). This way, an enhancement in SFG can turn into a suppression in DFG.

Probing field reversal in the time domain

In order to test out model, we used the 2.33 eV beam for DFG as pump beam and followed its effect on the surface nonlinear response by SFG. Fig. 5 plots the magnitude of the nonresonant background and of the pyridine resonance as a function of pump-probe time delay for a pyridine coverage of 1 ML. Figure 5 also demonstrates that the large change in nonresonant response is due to the presence of the adsorbate, as a bare copper surface shows a much smaller response. In fact, the transient effect gradually disappears with decreasing pyridine coverage as shown in the Fig. S5 of the supporting information. The transients depend approximately linearly on the power of the pump beam, as the inset to Fig. 5 shows.

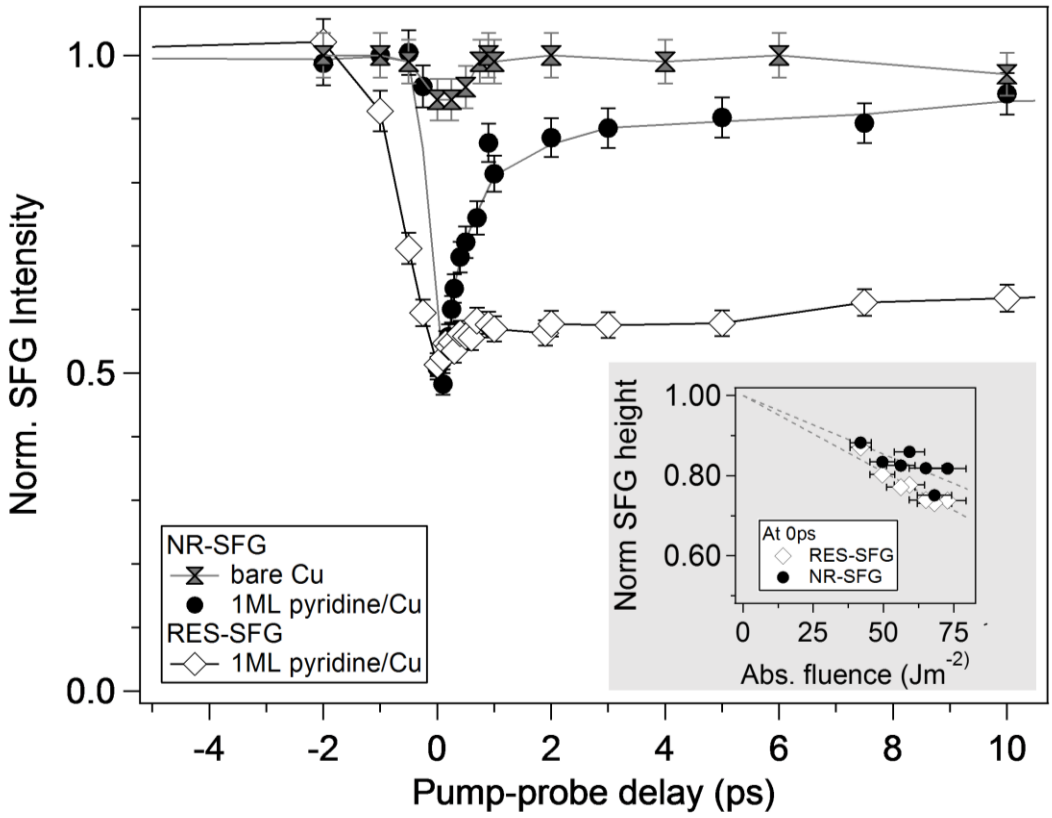

Figure 5. 2.33 eV-pump-probe results for 1 ML pyridine/Cu(110) at 100 K and bare Cu(110). Inset, fluence dependence of the RES- and NR-SFG at 0 ps pump delay.

The nonresonant magnitude is measured with a time resolution of ca. 400 fs, given by the cross correlation of IR and visible pump pulses, while the time resolution of resonant height and nonresonant phase is determined by the pyridine C-H vibrational the dephasing time, that is 2 ps for our typical 5 cm^{-1} line width. Both surface electrons and pyridine resonance exhibit a strong decrease on a comparable timescale, although they recover to unpumped values on very different timescales. The reduction of the resonant signal at long delay times is probably caused by a structural rearrangement in the pyridine layer following dipole reversal, which will be the subject of a forthcoming publication.

The reduction of the nonresonant background has a lifetime of approximately 460 fs and is therefore long-lived compared to a typical expectation of a few femtoseconds for the lifetime of an electronically excited state on a metal surface. A dipole-reversed excited state would however be stabilized by neighboring molecules in the ground state, since it induces an electric field in the same direction as the ground state. The attractive electrostatic interaction energy between a reversed dipole and its immediate neighbor can be estimated to be around 20 meV, if we assume a nearest neighbor distance of 5.1Å [7]. This is a lower limit, as the effect of a -1 D dipole will be felt over a 2 nm range[6], i.e. approximately 35 molecules in a (2×2) arrangement.

The reported second-order nonlinear response of pyridine adsorbed on Ag(110) in UHV could also be explained by our model[41]. At small coverages, where pyridine is thought to adsorb in a flat configuration, the second harmonic response to incoming 2.33 eV photons (well below Ag interband transitions) increases with coverage, while at high coverages, where N-bonded pyridine is thought to prevail, the SH signal was found to decrease to below the clean Ag(110) value. The initial enhancement might not be work-function related, since π-bonding of pyridine to silver could enhance the polarizability of the surface. However, the reduction of the signal below the clean surface value by N-bonded pyridine is very unusual. The work function reduction is less than on our Cu(110) surface ($\Delta\varphi$=-1.8 eV), but one would still expect a substantial static electric field and therefore enhancement of the second harmonic response. Since the predicted LUMO positions for pyridine on Cu(110) and Ag(110) are fairly similar[47], the pyridine LUMO could be within reach of the 2.33 eV exciting photon and the ensuing dipole moment reversal could lead to an overall reduction.

Since a wide range of aromatic molecules exhibit dipole moment reversal in the excited state[66] these experiments demonstrate the potential to alter the surface work function temporarily by photon excitation.

CONCLUSIONS

Pyridine adsorption on Cu(110) increases the surface dipole on the interface, lowering the work function by 2.9 eV. The high electric field generated on the pyridine-Cu interface plays an important role in the interpretation of the nonlinear optical response and we show that third order effects have to be taken into account. Comparison of SFG and DFG as a function of pyridine coverage shows that the local electric field can enhance the response as well as suppress it when an intense visible beam electronically excites pyridine and reverses its molecule dipole. The dipole reversal is relatively long-lived as shown by pump-probe experiments, revealing the potential for photon-induced work function manipulation.

ASSOCIATED CONTENT

Supporting Information. This material is available free of charge via the Internet at http://pubs.acs.org. The supporting information contains a compilation of the values of work function of pyridine on different metals (Table S1). The UPS of pyridine adsorption on Cu(110) (Fig. S1). The normalized pyridine on Cu(110) spectra for different coverages versus the collected spectra (Fig. S2). The spectral parameters for the two solutions fitted of the pyridine on Cu(110) (Fig. S3). The IR and Raman hyperolarizabilities calculated using Spartan (Table S2). The free-induction decay measurement for bare and 1 ML of pyridine on Cu(110) (Fig. S4) and the effect of the 2.33 eV-pump at different pyridine coverages on Cu(110) (Fig. S5).

AUTHOR INFORMATION

Corresponding Author

* e-mail: ngarciar@illinois.edu

* e-mail: Heike.Arnolds@liverpool.ac.uk

Present Addresses

[a] School of Chemical Sciences, Department of Chemistry, University of Illinois at Urbana-Champaign, Urbana, IL 61801, USA.

[b] Department of Chemistry, University of Surrey, Guildford, GU2 7XH, UK.

Author Contributions

MS and SJH performed the density functional calculations. NGR and HA designed, carried out the experiments, interpreted the data and wrote the manuscript. All authors have given approval to the final version of the manuscript.

Funding Sources

The research described in this study is based on work supported by the EPSRC under the awards EP/C011988/2 and EP/C01197X/2.

ACKNOWLEDGMENTS

We are grateful to EPSRC for equipment funding and a studentship for N.G.R. We thank I.M. McLeod and V.R. Dhanak for help with the UPS measurements, and A. Hodgson and F. McBride for providing the Kelvin probe.

REFERENCES

1. Heimel, G.; Romaner, L.; Zojer, E.; Brédas, J.-L., Toward Control of the Metal−Organic Interfacial Electronic Structure in Molecular Electronics: A First-Principles Study on Self-Assembled Monolayers of Π-Conjugated Molecules on Noble Metals. *Nano Lett.* **2007**, *7*, 932-940.

2. Ma, Z.; Rissner, F.; Wang, L.; Heimel, G.; Li, Q.; Shuai, Z.; Zojer, E., Electronic Structure of Pyridine-Based Sams on Flat Au(111) Surfaces: Extended Charge Rearrangements and Fermi Level Pinning. *Phys. Chem. Chem. Phys.* **2011**, *13*, 9747-9760.

3. Hofmann, O. T.; Deinert, J. C.; Xu, Y.; Rinke, P.; Stähler, J.; Wolf, M.; Scheffler, M., Large Work Function Reduction by Adsorption of a Molecule with a Negative Electron Affinity: Pyridine on ZnO(1010). *J. Chem. Phys.* **2013**, *139*, 174701.

4. Natan, A.; Kronik, L.; Haick, H.; Tung, R. T., Electrostatic Properties of Ideal and Non-Ideal Polar Organic Monolayers: Implications for Electronic Devices. *Adv. Mater.* **2007**, *19*, 4103-4117.

5. Monti, O. L. A., Understanding Interfacial Electronic Structure and Charge Transfer: An Electrostatic Perspective. *J. Phys. Chem. Lett.* **2012**, *3*, 2342-2351.

6. Kokalj, A., Electrostatic Model for Treating Long-Range Lateral Interactions between Polar Molecules Adsorbed on Metal Surfaces. *Phys. Rev. B* **2011**, *84*, 045418.

7. Deshlahra, P.; Conway, J.; Wolf, E. E.; Schneider, W. F., Influence of Dipole-Dipole Interactions on Coverage-Dependent Adsorption: CO and NO on Pt(111). *Langmuir* **2012**, *28*, 8408-8417.

8. Boxer, S. G., Stark Realities. *J. Phys. Chem. B* **2009**, *113*, 2972-2983.

9. Braunschweig, B.; Wieckowski, A., Surface Spectroscopy of Pt(1 1 1) Single-Crystal Electrolyte Interfaces with Broadband Sum-Frequency Generation. *J. Electroanal. Chem.* **2014**, *716*, 136-144.

10. Dreesen, L.; Humbert, C.; Celebi, M.; Lemaire, J. J.; Mani, A. A.; Thiry, P. A.; Peremans, A., Influence of the Metal Electronic Properties on the Sum-Frequency Generation Spectra of Dodecanethiol Self-Assembled Monolayers on Pt(111), Ag(111) Au(111) Single Crystals. *Appl. Phys. B* **2002**, *74*, 621-625.

11. Miyamae, T.; Takada, N.; Tsutsui, T., Probing Buried Organic Layers in Organic Light-Emitting Diodes under Operation by Electric-Field-Induced Doubly Resonant Sum-Frequency Generation Spectroscopy. *Appl. Phys. Lett.* **2012**, *101*.

12. Volpati, D.; Aoki, P. H. B.; Alessio, P.; Pavinatto, F. J.; Miranda, P. B.; Constantino, C. J. L.; Oliveira, O. N., Vibrational Spectroscopy for Probing Molecular-Level Interactions in Organic Films Mimicking Biointerfaces. *Adv. Colloid. Interface Sci.* **2014**, *207*, 199-215.

13. Wang, J.; Chen, X.; Clarke, M. L.; Chen, Z., Detection of Chiral Sum Frequency Generation Vibrational Spectra of Proteins and Peptides at Interfaces in Situ. *Proceedings of the National Academy of Sciences of the United States of America* **2005**, *102*, 4978-4983.

14. Zhang, C.; Myers, J. N.; Chen, Z., Elucidation of Molecular Structures at Buried Polymer Interfaces and Biological Interfaces Using Sum Frequency Generation Vibrational Spectroscopy. *Soft Matter* **2013**, *9*, 4738-4761.

15. Kawaguchi, T.; Shiratori, K.; Henmi, Y.; Ishiyama, T.; Morita, A., Mechanisms of Sum Frequency Generation from Liquid Benzene: Symmetry Breaking at Interface and Bulk Contribution. *J. Phys. Chem. C* **2012**, *116*, 13169-13182.

16. Yamaguchi, S.; Shiratori, K.; Morita, A.; Tahara, T., Electric Quadrupole Contribution to the Nonresonant Background of Sum Frequency Generation at Air/Liquid Interfaces. *J. Chem. Phys.* **2011**, *134*, 184705.

17. Guyot-Sionnest, P.; Tadjeddine, A., Study of Ag(111) and Au(111) Electrodes by Optical 2nd-Harmonic Generation. *J. Chem. Phys.* **1990**, *92*, 734-738.

18. Humbert, C.; Busson, B.; Tadjeddine, A., Enhanced Stability of a Carbon Monoxide Monolayer Adsorbed on Platinum under Electrochemical Control Probed by Sum-Frequency Generation Spectroscopy. *J. Phys. Chem. C* **2016**, *120*, 16211-16220.

19. Lan, S.; Rodrigues, S.; Cui, Y.; Kang, L.; Cai, W., Electrically Tunable Harmonic Generation of Light from Plasmonic Structures in Electrolytes. *Nano Lett.* **2016**, *16*, 5074-5079.

20. Geiger, F. M., Second Harmonic Generation, Sum Frequency Generation, and $X^{(3)}$: Dissecting Environmental Interfaces with a Nonlinear Optical Swiss Army Knife. *Annu. Rev. Phys. Chem.* **2009**, *60*, 61-83.

21. Eisenthal, K. B., Liquid Interfaces Probed by Second-Harmonic and Sum-Frequency Spectroscopy. *Chem. Rev.* **1996**, *96*, 1343-1360.

22. Ong, S.; Zhao, X.; Eisenthal, K. B., Polarization of Water Molecules at a Charged Interface: Second Harmonic Studies of the Silica/Water Interface. *Chem. Phys. Lett.* **1992**, *191*, 327-335.

23. Eftekhari-Bafrooei, A.; Borguet, E., Effect of Electric Fields on the Ultrafast Vibrational Relaxation of Water at a Charged Solid–Liquid Interface as Probed by Vibrational Sum Frequency Generation. *J, Phys. Chem. Lett.* **2011**, *2*, 1353-1358.

24. Sun, S.; Tian, C.; Shen, Y. R., Surface Sum-Frequency Vibrational Spectroscopy of Nonpolar Media. *Proceedings of the National Academy of Sciences* **2015**, *112*, 5883-5887.

25. Arnolds, H.; Symonds, J. P. R.; Zhang, V. L.; King, D. A., In Situ Characterization of Ultrafast Laser Pulses for Sum Frequency Surface Studies. *Rev. Sci. Instrum.* **2003**, *74*, 3943-3946.

26. Lagutchev, A.; Lozano, A.; Mukherjee, P.; Hambir, S. A.; Dlott, D. D., Compact Broadband Vibrational Sum-Frequency Generation Spectrometer with Nonresonant Suppression. *Spectrochim. Acta, Part A* **2010**, *75*, 1289-1296.

27. Perdew, J. P.; Chevary, J. A.; Vosko, S. H.; Jackson, K. A.; Pederson, M. R.; Singh, D. J.; Fiolhais, C., Atoms, Molecules, Solids, and Surfaces - Applications of the Generalized Gradient Approximation for Exchange and Correlation. *Phys. Rev. B* **1992**, *46*, 6671-6687.

28. Jones, G.; Jenkins, S. J., Water and Ammonia on Cu{110}: Comparative Structure and Bonding. *Phys. Chem. Chem. Phys.* **2013**, *15*, 4785-4798.

29. Monkhorst, H. J.; Pack, J. D., Special Points for Brillouin-Zone Integrations *Phys. Rev. B* **1976**, *13*, 5188-5192.

30. Bandy, B. J.; Lloyd, D. R.; Richardson, N. V., Selection-Rules in Photoemission from Adsorbates - Pyridine Adsorbed on Copper. *Surf. Sci.* **1979**, *89*, 344-353.

31. Lee, J. G.; Ahner, J.; Yates, J. T., The Adsorption Conformation of Chemisorbed Pyridine on the Cu(110) Surface. *J. Chem. Phys.* **2001**, *114*, 1414-1419.

32. Dougherty, D. B.; Lee, J.; Yates, J. T., Jr., Role of Conformation in the Electronic Properties of Chemisorbed Pyridine on Cu(110): An Stm/Sts Study. *J. Phys. Chem. B* **2006**, *110*, 11991-11996.

33. Bader, M.; Haase, J.; Frank, K.; Ocal, C.; Pushchmann, A., Near Edge X-Ray Absorption Fine-Structure Studies of Ring Molecules Adsorbed on Single-Crystal Surfaces. *Journal de Physique* **1986**, *47*, 491-496.

34. Gießel, T., et al., Adsorption Site and Orientation of Pyridine on Cu(110) Determined by Photoelectron Diffraction. *J. Chem. Phys.* **1999**, *110*, 9666-9672.

35. Quiniou, B.; Bulović, V.; Osgood, R., Observation of Image-Potential-Induced Resonances on Cu(110) Using the Two-Photon Photoemission Technique. *Phys. Rev. B* **1993**, *47*, 15890-15895.

36. Zhong, Q.; Gahl, C.; Wolf, M., Two-Photon Photoemission Spectroscopy of Pyridine Adsorbed on Cu(111). *Surf. Sci.* **2002**, *496*, 21-32.

37. Gland, J. L.; Somorjai, G. A., Low-Energy Electron-Diffraction and Work Function Studies of Benzene, Naphthalene and Pyridine Adsorbed on Pt(111) and Pt(100) Single-Crystal Surfaces. *Surf. Sci.* **1973**, *38*, 157-186.

38. Demore, B. B.; Wilcox, W. S.; Goldstein, J. H., Microwave Spectrum and Dipole Moment of Pyridine. *J. Chem. Phys.* **1954**, *22*, 876-877.

39. Nelson, R. D., Jr ; Lide, David R , Jr ; Maryott, Arthur A, Selected Values of Electric Dipole Moments for Molecules in the Gas Phase. *National Standard Reference Data Series* **1967**.

40. Poelsema, B.; Palmer, R. L.; Comsa, G., Helium Scattering and Work Function Investigation of CO Adsorption on Pt(111) and Vicinal Surfaces. *Surf. Sci.* **1982**, *123*, 152-164.

41. Heskett, D.; Urbach, L. E.; Song, K. J.; Plummer, E. W.; Dai, H. L., Oxygen and Pyridine on Ag(110) Studied by Second Harmonic Generation: Coexistence of Two Phases within Monolayer Pyridine Coverage. *Surf. Sci.* **1988**, *197*, 225 - 238.

42. Witte, G.; Lukas, S.; Bagus, P. S.; Wöll, C., Vacuum Level Alignment at Organic/Metal Junctions: "Cushion" Effect and the Interface Dipole. *Appl. Phys. Lett.* **2005**, *87*, 263502.

43. Bradshaw, A. M.; Scheffler, M., Lateral Interactions in Adsorbed Layers. *J. Vac. Sci. Technol.* **1979**, *16*, 447-454.

44. Maschhoff, B. L.; Cowin, J. P., Corrected Electrostatic Model for Dipoles Adsorbed on a Metal-Surface. *J. Chem. Phys.* **1994**, *101*, 8138-8151.

45. Topping, J., On the Mutual Potential Energy of a Plane Network of Doublets. *P. Roy. Soc. Lon. A Mat.* **1927**, *114*, 67-72.

46. Smith, N. V.; Chen, C. T.; Weinert, M., Distance of the Image Plane from Metal Surfaces. *Phys. Rev. B* **1989**, *40*, 7565-7573.

47. Atodiresei, N.; Caciuc, V.; Franke, J. H.; Blügel, S., Role of the Van Der Waals Interactions on the Bonding Mechanism of Pyridine on Cu(110) and Ag(110) Surface: First-Principles Study. *Phys. Rev. B* **2008**, *78*, 045411.

48. Le Rille, A.; Tadjeddine, A., In Situ Visible-Infrared Sum and Difference Frequency Generation at the Electrochemical Interface. *J. Electroanal. Chem.* **1999**, *467*, 238-248.

49. Tadjeddine, A.; Vidal, F., Chapter 9 - Vibrational and Electronic Spectroscopic Investigation of the Electrochemical Interface Using IR-Visible Sum-Frequency Generation and Related Nonlinear Optical Techniques. In *In-Situ Spectroscopic Studies of Adsorption at the Electrode and Electrocatalysis*, Sun, S.-G.; Christensen, P. A.; Wieckowski, A., Eds. Elsevier Science B.V.: 2007; pp 273-298.

50. Busson, B.; Tadjeddine, A., Non-Uniqueness of Parameters Extracted from Resonant Second-Order Nonlinear Optical Spectroscopies. *J. Phys. Chem. C* **2009**, *113*, 21895-21902.

51. Haq, S.; King, D. A., Configurational Transitions of Benzene and Pyridine Adsorbed on Pt{111} and Cu{110} Surfaces: An Infrared Study. *J. Phys. Chem.* **1996**, *100*, 16957-16965.

52. Gao, P.; Weaver, M. J., Vibrational Coupling Effects for Cyanide and Aromatic Adsorbates at Gold Electrodes: A Comparative Study Using Surface Raman and Infrared Spectroscopies. *J. Phys. Chem.* **1989**, *93*, 6205-6211.

53. Ikezawa, Y.; Sawatari, T.; Kitazume, T.; Hiroshi, G.; Toriba, K., In Situ FTIR Study of Pyridine Adsorbed on a Polycrystalline Gold Electrode. *Electrochim. Acta* **1998**, *43*, 3297-3301.

54. Johansson, P., Illustrative Direct Ab Initio Calculations of Surface Raman Spectra. *Phys. Chem. Chem. Phys.* **2005**, *7*, 475-482.

55. Verhoef, R. W.; Asscher, M., The Work Function of Adsorbed Alkalis on Metals Revisited: A Coverage-Dependent Polarizability Approach. *Surf. Sci.* **1997**, *391*, 11-18.

56. Rosenzweig, Z.; Asscher, M., Optical Second-Harmonic Generation from Surfaces as a Monitor for Adsorbate Induced Work Function Changes. *Surf. Sci.* **1988**, *204*, L732-L738.

57. Grubb, S. G.; DeSantolo, A. M.; Hall, R. B., Optical Second-Harmonic Generation Studies of Molecular Adsorption on Platinum (111) and Nickel (111). *J. Phys. Chem.* **1988**, *92*, 1419-1425.

58. Schwab, C.; Meister, G.; Woll, J.; Gerlach, A.; Goldmann, A., Experimental Intensity Analysis of Second Harmonic Generation at the Cu(110) Surface. *Surf. Sci.* **2000**, *457*, 273-284.

59. Frank, K. H.; Dudde, R.; Koch, E. E., Electron-Affinity Levels of Benzene and Azabenzenes on Cu(111) and Au(110) Revealed by Inverse Photoemission. *Chem. Phys. Lett.* **1986**, *132*, 83-87.

60. Matranga, C.; Guyot-Sionnest, P., Absolute Intensity Measurements of the Optical Second-Harmonic Response of Metals from 0.9 to 2.5 eV. *J. Chem. Phys.* **2001**, *115*, 9503-9512.

61. Petrocelli, G.; Martellucci, S.; Francini, R., Wavelength Dependence of Second-Harmonic Generation at the Copper Surface. *Appl. Phys. A* **1993**, *56*, 263-266.

62. Metzger, B.; Gui, L.; Giessen, H., Ultrabroadband Chirped Pulse Second-Harmonic Spectroscopy: Measuring the Frequency-Dependent Second-Order Response of Different Metal Films. *Opt. Lett.* **2014**, *39*, 5293-5296.

63. Luce, T. A.; Bennemann, K. H., Nonlinear Optical Response of Noble Metals Determined from First-Principles Electronic Structures and Wave Functions: Calculation of Transition Matrix Elements. *Phys. Rev. B* **1998**, *58*, 15821-15826.

64. Jug, K.; Hahn, G., Properties of Excited States of Aromatic Rings Containing Nitrogen. *J. Comput. Chem.* **1983**, *4*, 410-418.

65. Hochstrasser, R. M.; Klimcak, C. M., Stark Modulation of the Electronic Spectrum of Pyridine in Benzene at 1.6 K. *Chem. Phys. Lett.* **1978**, *53*, 429-432.

66. Rosenberg, M.; Dahlstrand, C.; Kilså, K.; Ottosson, H., Excited State Aromaticity and Antiaromaticity: Opportunities for Photophysical and Photochemical Rationalizations. *Chem. Rev.* **2014**, *114*, 5379-5425.

TABLE OF CONTENTS